



Delft University of Technology

A hybrid segmentation method for partitioning the liver based on 4D DCE-MR images

Zhang, Tian; Wu, Zhiyi; Runge, Jurgen H.; Lavini, Cristina; Stoker, Jaap; Van Gulik, Thomas; Cieslak, Kasia P.; Van Vliet, Lucas J.; Vos, Frans M.

DOI

[10.1117/12.2293530](https://doi.org/10.1117/12.2293530)

Publication date

2018

Document Version

Final published version

Published in

Medical Imaging 2018

Citation (APA)

Zhang, T., Wu, Z., Runge, J. H., Lavini, C., Stoker, J., Van Gulik, T., Cieslak, K. P., Van Vliet, L. J., & Vos, F. M. (2018). A hybrid segmentation method for partitioning the liver based on 4D DCE-MR images. In *Medical Imaging 2018: Image Processing* (Vol. 10574). Article 1057434 SPIE. <https://doi.org/10.1117/12.2293530>

Important note

To cite this publication, please use the final published version (if applicable). Please check the document version above.

Copyright

Other than for strictly personal use, it is not permitted to download, forward or distribute the text or part of it, without the consent of the author(s) and/or copyright holder(s), unless the work is under an open content license such as Creative Commons.

Takedown policy

Please contact us and provide details if you believe this document breaches copyrights. We will remove access to the work immediately and investigate your claim.

PROCEEDINGS OF SPIE

SPIEDigitalLibrary.org/conference-proceedings-of-spie

A hybrid segmentation method for partitioning the liver based on 4D DCE-MR images

Tian Zhang, Zhiyi Wu, Jurgen H. Runge, Cristina Lavini, Jaap Stoker, et al.

Tian Zhang, Zhiyi Wu, Jurgen H. Runge, Cristina Lavini, Jaap Stoker, Thomas van Gulik, Kasia P. Cieslak, Lucas J. van Vliet, Frans M. Vos, "A hybrid segmentation method for partitioning the liver based on 4D DCE-MR images," Proc. SPIE 10574, Medical Imaging 2018: Image Processing, 1057434 (2 March 2018); doi: 10.1117/12.2293530

SPIE.

Event: SPIE Medical Imaging, 2018, Houston, Texas, United States

A Hybrid Segmentation Method for Partitioning the Liver Based on 4D DCE-MR Images

Tian Zhang^a, Zhiyi Wu^a, Jurgen H. Runge^b, Cristina Lavini^b, Jaap Stoker^b,
Thomas van Gulik^c, Kasia P. Cieslak^c, Lucas J. van Vliet^a, Frans M. Vos^{a,b}

^aQuantitative Imaging Group, Department of Imaging Physics, Delft University of Technology, Delft, The Netherlands

^bDepartment of Radiology, Academic Medical Center Amsterdam, Amsterdam, The Netherlands

^cDepartment of Surgery, Academic Medical Center Amsterdam, Amsterdam, The Netherlands

ABSTRACT

The Couinaud classification of hepatic anatomy partitions the liver into eight functionally independent segments. Detection and segmentation of the hepatic vein (HV), portal vein (PV) and inferior vena cava (IVC) plays an important role in the subsequent delineation of the liver segments. To facilitate pharmacokinetic modeling of the liver based on the same data, a 4D DCE-MR scan protocol was selected. This yields images with high temporal resolution but low spatial resolution. Since the liver's vasculature consists of many tiny branches, segmentation of these images is challenging. The proposed framework starts with registration of the 4D DCE-MRI series followed by region growing from manually annotated seeds in the main branches of key blood vessels in the liver. It calculates the Pearson correlation between the time intensity curves (TICs) of a seed and all voxels. A maximum correlation map for each vessel is obtained by combining the correlation maps for all branches of the same vessel through a maximum selection per voxel. The maximum correlation map is incorporated in a level set scheme to individually delineate the main vessels. Subsequently, the eight liver segments are segmented based on three vertical intersecting planes fit through the three skeleton branches of HV and IVC's center of mass as well as a horizontal plane fit through the skeleton of PV. Our segmentation regarding delineation of the vessels is more accurate than the results of two state-of-the-art techniques on five subjects in terms of the average symmetric surface distance (ASSD) and modified Hausdorff distance (MHD). Furthermore, the proposed liver partitioning achieves large overlap with manual reference segmentations (expressed in Dice Coefficient) in all but a small minority of segments (mean values between 87% and 94% for segments 2-8). The lower mean overlap for segment 1 (72%) is due to the limited spatial resolution of our DCE-MR scan protocol.

Keywords: Functional liver segments, time intensity curve (TIC), Couinaud classification, level set, DCE-MRI.

1. INTRODUCTION

During liver surgery, resection of lesions inevitably goes at the expense of healthy hepatocyte tissue. To reduce this loss as much as possible and to limit the mortality rates after surgery, the Couinaud classification of liver anatomy was introduced¹. This classification system partitions the liver into eight segments such that each of them has an independent circulatory system. It targets resecting only that segment in which the tumor is localized, without damaging the liver parenchyma of adjacent segments².

Conventionally, radiologists apply the Couinaud classification by manually annotating vessels in the liver, which is tedious, time-consuming and prone to errors. Accurate automatic methods for segmenting vessels are desired to improve the time efficiency. Several segmentation methods have been proposed, especially for X-ray computed tomography (CT) images which have relatively high spatial resolution³⁻⁴. However, the problem remains unsolved when it comes to magnetic resonance (MR) images, which is likely related to the lower spatial resolution of MR compared to CT imaging.

In this paper, we introduce a segmentation framework partitioning the liver according to Couinaud's classification of liver anatomy based on 4D dynamic contrast-enhanced magnetic resonance imaging (DCE-MRI) data. These data have high temporal resolution, but limited spatial resolution. We will show that our framework facilitates the segmentation of the liver vessels and in turn enables the segmentation of the eight liver segments.

2. METHODOLOGY

DCE-MRI data were acquired on a 3T Philips scanner via a 3D SPGR sequence. The x-axis of the data corresponds to the anterior-posterior direction, the y-axis to the left-right direction and the z-axis to the superior-inferior direction. The acquisition parameter settings were TE/TR = 2.3/3.75 ms, FA = 15 °; matrix size = 128×128×44, voxel size = 3×3×5 mm³, acquisition time = 2.141 s for each volume; sampling interval (between images) was 2.141 s for volumes 1-81, 30 s for volumes 82-98, and 60 s for volumes 99-108. The total imaging time was approximately 20 minutes.

2.1 Registration

To achieve spatial correspondence between corresponding voxels of the data, each 4D DCE-MR image series is registered to the last dynamic volume. In order to do so, we apply the Modality Independent Neighborhood Descriptor (MIND) method⁵, which is a state-of-the-art technique for multi-modal image registration. Essentially, it relies on a patch-based descriptor of the structure in a local neighborhood:

$$MIND(I, \mathbf{x}, \mathbf{r}) = \frac{1}{n} \exp \left(- \frac{D_p(I, \mathbf{x}, \mathbf{x} + \mathbf{r})}{V(I, \mathbf{x})} \right) \quad (1)$$

in which I is an image, \mathbf{r} is an offset in neighborhood R of size $R \times R$ around position \mathbf{x} and n a normalization constant; D_p is the distance between two image patches, measured by the sum of squared differences (SSD):

$$D_p(I, \mathbf{x}_1, \mathbf{x}_2) = \sum_{\mathbf{p} \in P} (I(\mathbf{x}_1 + \mathbf{p}) - I(\mathbf{x}_2 + \mathbf{p}))^2 \quad (2)$$

and $V(I, \mathbf{x})$ is the mean of the patch distances in a small neighborhood N :

$$V(I, \mathbf{x}) = \frac{1}{num(N)} \sum_{\mathbf{p} \in P} D_p(I, \mathbf{x}, \mathbf{x} + \mathbf{p}) \quad (3)$$

MIND registration can be described as

$$\mathbf{u}^* = \arg \min_{\mathbf{u}} \left\{ \sum_{\mathbf{x}} \left[\frac{1}{|R|} \sum_{\mathbf{r} \in R} |MIND(I, \mathbf{x}, \mathbf{r}) - MIND(J, \mathbf{x}, \mathbf{r})| \right] + \alpha |\nabla \mathbf{u}(\mathbf{x})|^2 \right\} \quad (4)$$

where $\mathbf{u} = (u, v, w)$ is the deformation field and α a coefficient that weighs a regularization term. In this paper we follow the default setup as introduced in ref.⁵: $R = 3$, $N = N_6$ i.e. a six-connected neighborhood, patch size $D = 3$, and the regularization coefficient $\alpha = 0.1$.

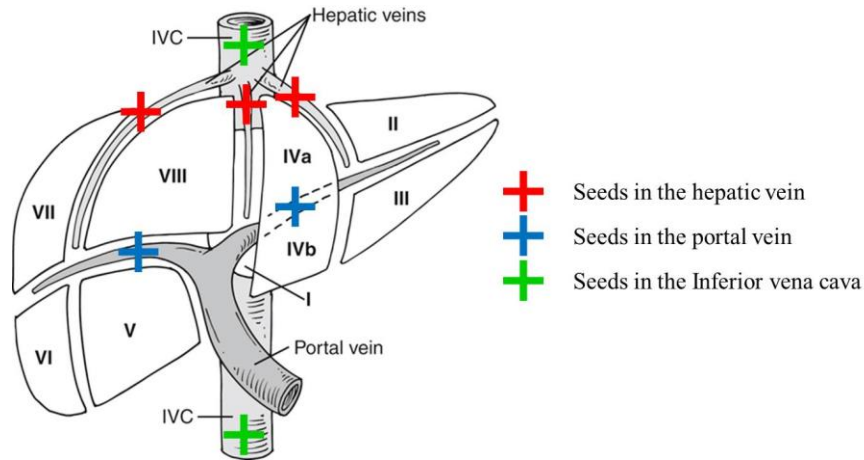


Figure 1. Locations of seed points in the hepatic vein (HV), portal vein (PV) and inferior vena cava (IVC).

2.2 Segmentation of the hepatic vasculature

The Couinaud classification partitions the liver in functionally independent segments based on the vasculature. Our method resembles this standard method, but relies on a semi-automatic segmentation of the key liver vessels. Specifically, a region growing method is applied to the 4D MR images to segment the main blood vessels as well as the liver. It adopts Pearson correlation between the time intensity curves (TICs) as distance metric⁶. Therefore, seeds are manually placed in the main branches of the liver's vasculature: hepatic vein (HV), portal vein (PV), and in the inferior vena cava (IVC), see Figure 1⁷. Since the blood in each main vessel has taken a different route through the human body, the TIC from each seed point is different. From each such seed the TIC is correlated with the entire 4D volume of TIC curves.

Subsequently, the maximum correlation is determined over the correlation maps for key vessel (HV, PV and IVC). As such, for each key vessel a separate maximum correlation map is obtained. Thereafter, the hybrid levelset segmentation method proposed by Y. Zhang et al.⁸ is separately applied to the three maximum correlation maps. It takes boundary as well as region information into consideration while minimizing the next data term

$$E(\phi) = -\int_{\Omega} (I - \mu)H(\phi) d\Omega + \beta \int_{\Omega} g |\nabla H(\phi)| d\Omega \quad (5)$$

where I is the image, g represents the gradient of the image, β is a weighting coefficient, $H(\phi)$ is the Heaviside function, μ is a parameter that represents the lower bound of the gray-level in the segmented object. The level set method is initiated by small spheres placed at the seed points. As such, a region growing method is applied to segment the hepatic vein (HV), portal vein (PV) and inferior vena cava (IVC). In addition, the first dynamic image is subtracted from the last dynamic image of the registered DCE-MRI series. Subsequently, the liver is segmented based on the resulting "contrast" volume by means of a level set approach⁹.

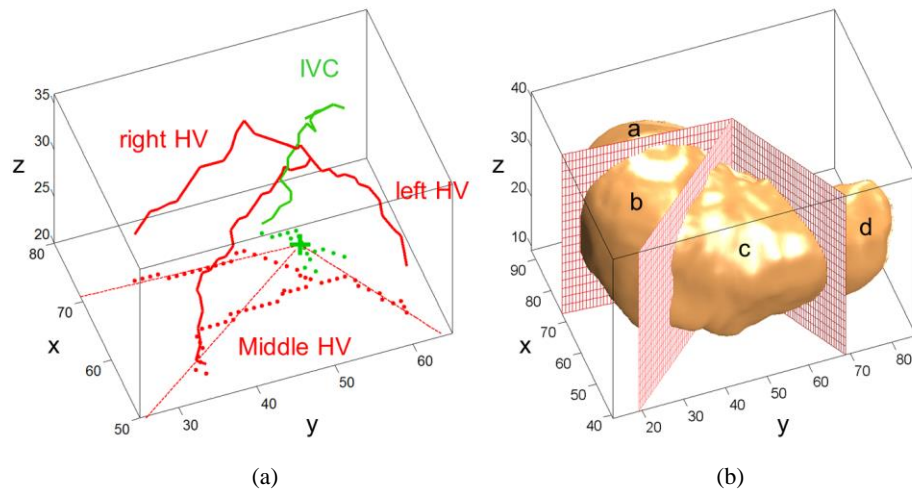


Figure 2. (a) The skeletons of left, middle, right HVs and IVC obtained by thinning the segmented structures. The red and green dashed points represent the coordinates of HVs and IVC projected onto the xy -plane. The green, cross-shaped symbol denotes the IVC's projected center of mass; (b) the three vertical planes dividing the liver into four parts; the lobes labeled a-d are defined as right posterior section, right anterior section, left medial section and left lateral section, respectively.

2.3 Definition of hepatic segments

In order to delineate the liver segments, skeletons representing the vessels are obtained by parallel medial axis thinning as described in ref.¹⁰. Example skeletons of the hepatic vein (HV), portal vein (PV) and inferior vena cava (IVC) are shown in Figure 2 (a) and Figure 3 (a). The partitioning of the liver is carried out according to Couinaud's classification using intersegmental planes¹¹. For the vertical partitioning, i.e. along the scan's z -axis, three planes spanned by the three main branches of HV were defined respectively. They can be generally expressed as

$$Ax + By = 1. \quad (6)$$

In Figure 2 (a), the HVs and the IVC are projected onto the xy -plane. For each HV branch, equation (6) is fit through the projected skeleton points and the IVC's center of mass. These are depicted by respectively the red dashed points and green cross-shaped point in Figure 2 (a). As such, the liver is divided into four lobes as shown in Figure 2 (b).

The skeleton of the PV is shown in Figure 3 (a). A horizontal plane fit through the PV's skeleton divides the superior and inferior liver lobes, as show in Figure 3 (b).

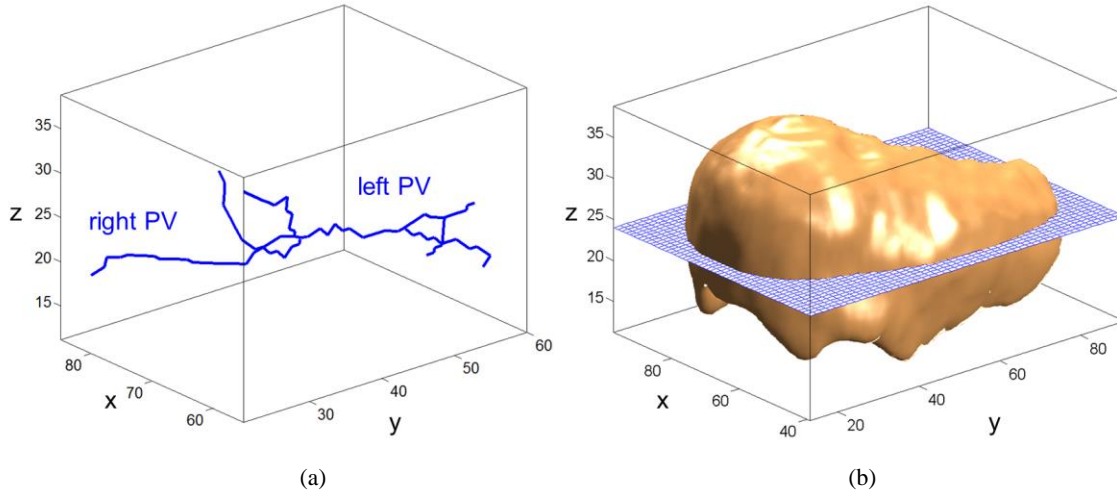


Figure 3. (a) The skeleton of the PV; (b) liver partitioning by fitting a horizontal plane.

In Couinaud's classification, the first segment is roundish and located around the region between the HV and IVC. However, the border between segment 1 and the other segments is not visible in our DCE-MR images due to the low spatial resolution. Therefore, the combination of half a sphere and cylinder is adopted to model the shape of segment 1. The modeling procedure is illustrated in Figure 4. In the horizontal resection plane, an inscribing sphere is defined centered at the projected IVC's center of mass and with a radius equal to the distance between the IVC's center of mass and the nearest point on the PV skeleton. Subsequently, a cylinder with the same radius as the sphere extends from the sphere in the positive y -direction. The cylindrical segment thus delineated is truncated by the border of the liver mask obtained as described below equation (5). The extended sphere is also truncated by the vertical plane as indicated in Figure 4 (a).

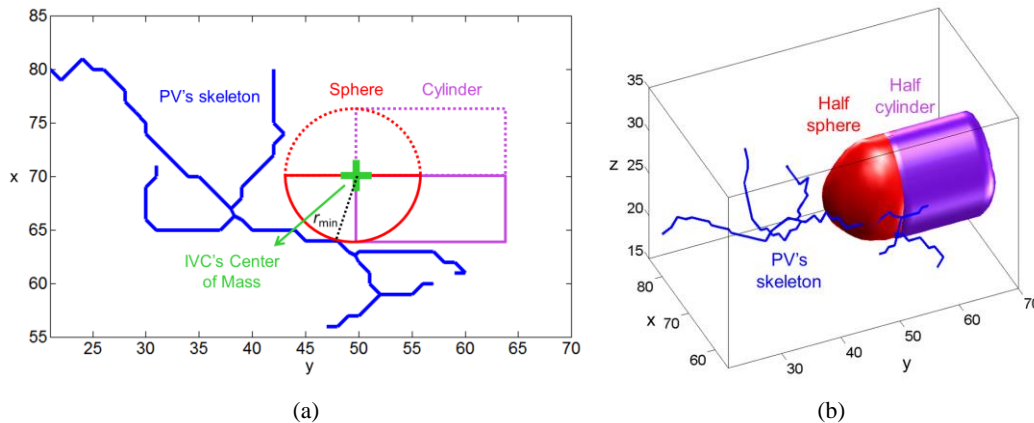


Figure 4. Modeling of liver segment 1. (a) An inscribing sphere is defined centered at the IVC's projected center-of-mass (on the horizontal plane from Figure 3), whose radius is determined by the nearest point of the PV skeleton. The sphere was extended by a cylindrical segment of the same radius in the positive y -direction. The red and purple solid lines indicate the half (of the sphere and cylinder) that is kept while the dashed lines correspond to the half that is removed; (b) the illustration of the kept half sphere and cylinder. Their combination is the final model to identify liver segment 1.

Table 1. Conditions delineating the liver segments. A and B : constant parameters for each plane definition. L : left, R : right, LHV : left hepatic vein, MHV : middle hepatic vein, RHV : right hepatic vein, PV : portal vein, IVC 's CM : IVC 's center of mass in the horizontal resection plane. r_{min} : the distance between IVC 's center of mass and the nearest point on PV 's skeleton.

Segment	Defining conditions
1	$(x^2 + y^2 + z^2 < r_{min}^2 \mid y^2 + z^2 < r_{min}^2) \& x < x_{IVC's\ CM}$
2	$A_{LHV}x + B_{LHV}y > 1 \& z > z_{PV}$
3	$A_{LHV}x + B_{LHV}y > 1 \& z < z_{PV}$
4	$A_{LHV}x + B_{LHV}y < 1 \& A_{MHV}x + B_{MHV}y < 1$
5	$A_{RHV}x + B_{RHV}y < 1 \& A_{MHV}x + B_{MHV}y > 1 \& z < z_{PV}$
6	$A_{RHV}x + B_{RHV}y > 1 \& z < z_{PV}$
7	$A_{RHV}x + B_{RHV}y > 1 \& z > z_{PV}$
8	$A_{RHV}x + B_{RHV}y < 1 \& A_{MHV}x + B_{MHV}y > 1 \& z > z_{PV}$

Table 1 summarizes the conditions to define the eight liver segments. Each segment consists of voxel points (x, y, z) , which satisfy the corresponding conditions. The first segment was calculated and excluded before the other segments were determined.

3. RESULTS

Figure 5 shows the correlation map for each branch of the hepatic vein. Note that each branch obtains the highest correlation in its individual map. As a result, the maximum selection map gets the highest contrast of the hepatic vein from a global point of view. The portal vein and inferior vena cava are processed in the same way.

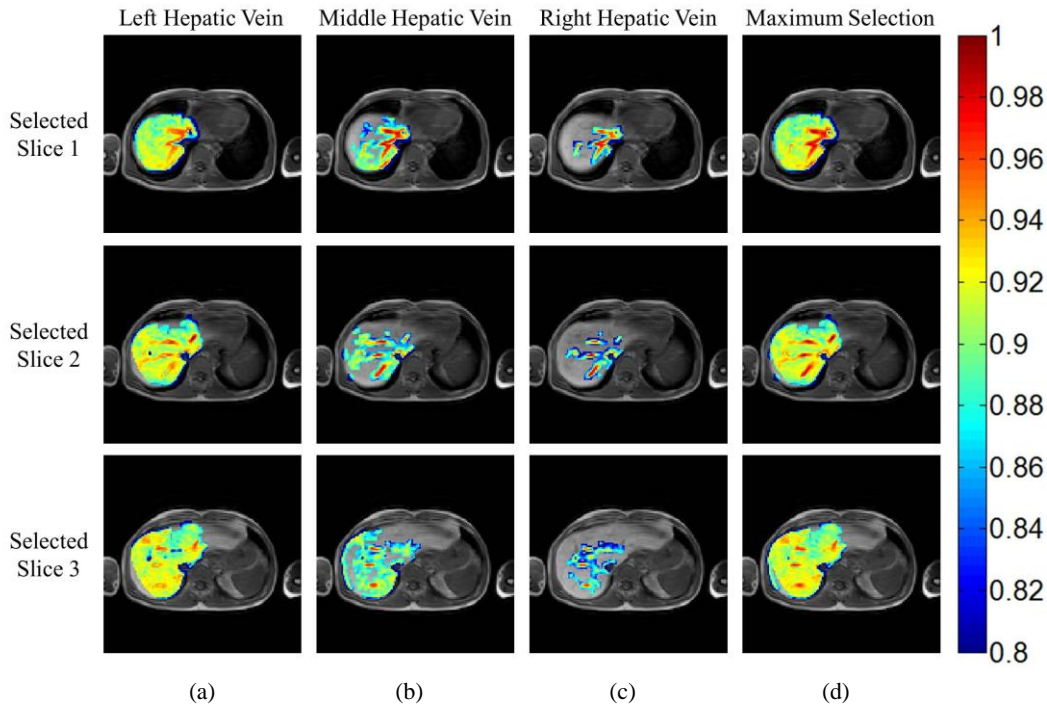


Figure 5. (a)-(c):Correlation maps in three slices of the left, middle and right hepatic veins, respectively; (d) The HV maximum correlation map composed by voxel-based maximum selection of correlation maps (a)-(c).

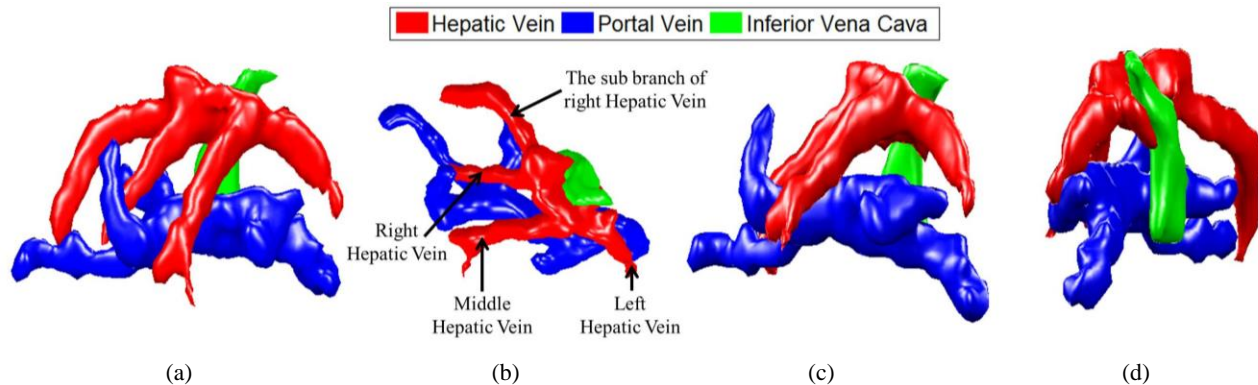


Figure 6. The segmentation of hepatic vein, portal vein and inferior vena cava in one subject. (a) Normal view; (b) top view; (c) front view; (d) side view.

Figure 6 shows the segmentation of the three key vessels from the liver as obtained by the aforementioned level set method. The vessels were also segmented by means of two state-of-the-art techniques, based on respectively a vesselness enhancement filter (VEF)¹² and a diffusion enhancing filter (DEF)⁴. An experienced radiologist manually delineated the vessels, which served as the reference standard. The accuracy of the semi-automatic methods was evaluated by means of the average symmetric surface distance (ASSD) and modified Hausdorff distance (MHD) on data of five subjects as shown in Table 2. The ASSD and MHD were calculated according to the following equations:

$$ASSD = \frac{\sum_{a \in A} \min_{b \in M} \|a - b\| + \sum_{b \in M} \min_{a \in A} \|a - b\|}{2(N_A + N_M)} \quad (7)$$

$$MHD(A, B) = \max \left\{ \frac{1}{N_A} \sum_{a \in A} \min_{b \in M} \|a - b\|, \frac{1}{N_M} \sum_{b \in M} \min_{a \in A} \|a - b\| \right\} \quad (8)$$

Table 2 collates the outcome of this experiment. Since both VEF and DEF are enhancement filter based segmentation methods, they cannot differentiate between different types of vessels such as HV, PV and IVC. For the sake of fairness, the segmentations of HV, PV and IVC obtained by our method are combined into a single segmentation to compare with the result produced by the two state-of-the-art methods. Apparently, our proposed method performs better in all five cases.

Table 2. Average symmetric surface distance (ASSD) and modified Hausdorff distance (MHD) of vessels segmented from five clinical cases with the proposed hybrid method and two standard techniques compared to manually annotated reference segmentations. VEF stands for a method based on a vesselness enhancement filter; DEF represents a diffusion enhancement filter (DEF) based technique. The numbers printed in boldface are the best result per row. All measures are in mm.

Metric	ASSD			MHD		
	VEF	DEF	Our method	VEF	DEF	Our method
Case 1	6.004	5.246	4.206	8.496	6.145	4.254
Case 2	6.351	6.155	5.580	9.668	8.885	6.894
Case 3	6.619	7.769	6.560	9.883	9.409	6.808
Case 4	9.069	6.123	5.271	14.327	8.410	7.828
Case 5	7.534	9.201	6.399	12.142	13.392	7.616
Average	7.115	6.899	5.603	10.903	9.248	6.680

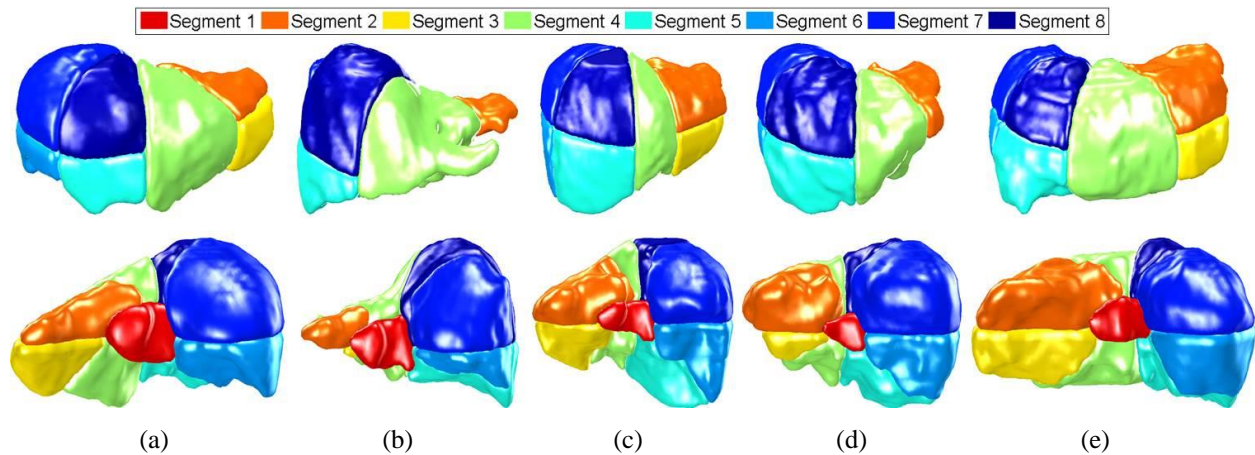


Figure 7. Visualization of eight functional liver segments from five subjects. (a)-(e) represent subject 1-5, respectively. Images in the first row give the front view while in the second row give the back view.

Table 3. The Dice Coefficient (DC) of volumetric overlap between the result of the proposed method and the manual segmentation.

DC (%)	Segment 1	Segment 2	Segment 3	Segment 4	Segment 5	Segment 6	Segment 7	Segment 8
Case 1	79.25	92.89	91.34	86.40	86.76	93.68	90.95	77.90
Case 2	77.34	87.85	64.44	92.44	91.72	85.84	92.83	94.26
Case 3	68.84	92.40	95.19	85.81	92.35	88.70	93.84	91.27
Case 4	59.49	89.36	90.28	91.24	92.34	90.40	96.42	95.06
Case 5	76.88	96.23	94.54	95.03	93.67	92.38	96.01	93.42
Average	72.36	91.75	87.16	90.18	91.37	90.20	94.01	90.38

After segmentation of the key vessels, the functional liver segments are delineated by applying the method described in 2.3. In Figure 7, the eight segments of five subjects are visualized. Additionally, the proposed segmentations are compared with manual ones, which are annotated under the supervision of one experienced radiologist in Table 3. It shows that the proposed segmentation method achieves good results in all but a small minority of cases, particularly concerning segment 1.

4. SUMMARY AND CONCLUSION

The hybrid segmentation method proposed by us for partitioning the liver from DCE-MRI images consists of two steps. In the first step, a region growing method is applied to segment the hepatic vein (HV), the portal vein (PV) and inferior vena cava (IVC) from the liver. In the second step, skeletons of these segmented vessels are regarded as landmarks to partition functional liver segments. Comparison with state-of-the-art methods shows that our method produces more accurate segmentations of the vessels in the liver. Moreover, our segmentations of functional liver segment have large overlap (measured through the Dice Coefficient) with a manually annotated reference. The proposed segmentation method can easily be adapted to other DCE-MRI or DCE-CT applications with low spatial resolutions.

REFERENCES

- [1] Couinaud, C., *Le foie: { études anatomiques et chirurgicales*, Masson & Cie (1957).
- [2] Pauli, E. M., Staveley-O'Carroll, K. F., Brock, M. V., Efron, D. T., Efron, G., "A handy tool to teach segmental liver anatomy to surgical trainees," *Arch. Surg.* 147(8), 692–693, American Medical Association (2012).
- [3] Chen, Y., Yue, X., Zhong, C., Wang, G., "Functional Region Annotation of Liver CT Image Based on Vascular Tree," *Biomed Res. Int.* 2016 (2016).

- [4] Luu, H. M., Klink, C., Moelker, A., Niessen, W., Walsum, T. van., "Quantitative evaluation of noise reduction and vesselness filters for liver vessel segmentation on abdominal {CTA} images," *Phys. Med. Biol.* 60(10), 3905 (2015).
- [5] Heinrich, M. P., Jenkinson, M., Bhushan, M., Matin, T., Gleeson, F. V., Brady, S. M., Schnabel, J. A., "MIND: Modality independent neighbourhood descriptor for multi-modal deformable registration," *Med. Image Anal.* 16(7), 1423–1435 (2012).
- [6] Lu, Y., Jiang, T., Zang, Y., "Region growing method for the analysis of functional MRI data," *Neuroimage* 20(1), 455–465 (2003).
- [7] "Liver | Clinical Gate.," <<https://clinicalgate.com/liver-3/>> (6 August 2017).
- [8] Zhang, Y., Matuszewski, B. J., Shark, L.-K., Moore, C. J., "Medical Image Segmentation Using New Hybrid Level-Set Method," 2008 Fifth Int. Conf. Biomed. Vis. Inf. Vis. Med. Biomed. Informatics, 71–76 (2008).
- [9] Zhang, T., Li, Z., Runge, J. H., Lavini, C., Stoker, J., van Gulik, T., van Vliet, L. J., Vos, F. M., "Improved registration of DCE-MR images of the liver using a prior segmentation of the region of interest," *Proc. SPIE* 9784, 978443–978448 (2016).
- [10] Lee, T.-C., Kashyap, R. L., Chu, C.-N., "Building skeleton models via 3-D medial surface axis thinning algorithms," *CVGIP Graph. Model. Image Process.* 56(6), 462–478, Elsevier (1994).
- [11] Fat-kin Yan., "Automatic Segmentation of Functional Hepatic Segments on Computed Tomography," University of Hong Kong (2011).
- [12] Jerman, T., Pernus, F., Likar, B., Spiclin, Z., "Enhancement of Vascular Structures in 3D and 2D Angiographic Images," *IEEE Trans. Med. Imaging* 35(9), 2107–2118 (2016).